



## Quantification of CO<sub>2</sub> and CH<sub>4</sub> emissions over Sacramento, California based on divergence theorem using aircraft measurements

5 Ju-Mee Ryoo<sup>1,2</sup>, Laura T. Iraci<sup>1</sup>, Tomoaki Tanaka<sup>1,8</sup>, Josette E. Marrero<sup>1,9</sup>, Emma L. Yates<sup>1,3</sup>,  
Inez Fung<sup>4,5</sup>, Anna M. Michalak<sup>6</sup>, Jovan Tadić<sup>6,7</sup>, Warren Gore<sup>1</sup>, T. Paul Bui<sup>1</sup>, Jonathan M.  
Dean-Day<sup>1,3</sup>, Cecilia S. Chang<sup>1,3</sup>

<sup>1</sup>Atmospheric Science Branch, NASA Ames Research Center, Moffett Field, CA, 94035

10 <sup>2</sup>Science and Technology Corporation (STC), Moffett Field, CA, 94035

<sup>3</sup>Bay Area Environmental Research Institute, Moffett Field, CA, 94035

<sup>4</sup>Department of Earth and Planetary Sciences, University of California, Berkeley, Berkeley, CA 94720

<sup>5</sup>Department of Environmental Sciences, Policy and Management, University of California, Berkeley, Berkeley, CA 94720

15 <sup>6</sup>Department of Global Ecology, Carnegie Institution for Science, Stanford, CA 94305

<sup>7</sup>Now at Climate and Ecosystem Sciences Division, Lawrence Berkeley National Laboratory, Berkeley, CA 94720

<sup>8</sup>Now at Japan Weather Association, Tokyo, Japan

<sup>9</sup>Now at Sonoma Technology, Inc., Petaluma, CA, 94954

20

Submitted to

25

*Atmospheric Measurement Techniques*

30

35

40 *Correspondence to:* Ju-Mee Ryoo ([ju-mee.ryoo@nasa.gov](mailto:ju-mee.ryoo@nasa.gov))



## Abstract

Emission estimates of carbon dioxide (CO<sub>2</sub>) and methane (CH<sub>4</sub>) and the meteorological factors affecting them are investigated over Sacramento, California, using an aircraft equipped with a cavity ring-down greenhouse gas  
45 sensor as part of the Alpha Jet Atmospheric eXperiment (AJAX) project. To better constrain the emissions fluxes, we designed flights in a cylindrical pattern and computed the emission fluxes from three flights using a kriging method and Gauss's divergence theorem.

The CO<sub>2</sub> and CH<sub>4</sub> mixing ratios at the downwind side of Sacramento show relatively consistent patterns across the three flights, but the fluxes vary - as a function of different wind patterns on a given flight day. The wind  
50 variability, seasonality, and assumptions about background concentrations affect the emissions estimates, by a factor of 1.5 to 8. The uncertainty is also impacted by meteorological conditions and distance from the emissions sources. The largest CH<sub>4</sub> mixing ratio was found over a local landfill.

The importance of vertical mass transfer for flux estimates is examined, but the difference in the total emission estimate with and without vertical mass transfer is found to be small, especially at the local scale. The total flux  
55 estimates accounting for the entire circumference are larger than those based solely on the downwind region. This indicates that a closed-shape flight profile can better contain total emissions relative to one-sided curtain flight because most cities have more than one point source and wind direction can change with time and altitude. To reduce the uncertainty of the emissions estimate, it is important that the sampling and modeling strategy account not only for known source locations but also possible unidentified sources around the city. Our results highlight that  
60 aircraft-based measurements using a closed shape flight pattern are an efficient and useful strategy for identifying emission sources and estimating local and city-scale greenhouse gas emission fluxes.



## 1. Introduction

65 The ability to obtain accurate emissions estimates of greenhouse gases has been highlighted as an important  
issue for many decades, not only for regulating local air quality but also for assessing national-scale air quality and  
greenhouse gas emissions. In particular, urban emissions need to be well-understood because approximately 70 % of  
anthropogenic greenhouse gas emissions originate from urban areas (International Energy Agency, 2008; Gurney et  
al., 2009, 2015). This often gives rise to *urban domes* with higher greenhouse gas (GHG) mixing ratios than  
70 surrounding areas (Oke, 1982; Idso et al., 1998, 2002; Koerner and Klopatek, 2002; Grimmond et al., 2004; Pataki  
et al., 2007; Andrews, 2008; Kennedy et al., 2009; Strong et al., 2011). Therefore, estimating greenhouse gas  
emissions at regional to national scales requires an improved understanding of urban GHG emissions and the role of  
human behavior in altering these emissions (Rosenzweig et al., 2010; Wofsy et al., 2010a, b).

The commonly used *bottom-up* inventories derive estimates of direct and indirect emissions of greenhouse  
75 gases based on an understanding of emission factors from the constituent sectors (Andres et al., 1999; Marland et al.,  
1985; Boden et al., 2010; California Air Resources Board, 2015; US EPA, 2016). These estimates rely on monthly  
or quarterly statistical averages of emission activities and often time-invariant emission factors, which mask  
behavioral patterns. However, recent *bottom-up* inventory data have improved from coarse estimates by using proxy  
data to produce fine spatial resolution estimates using specific activity data and emission factors corresponding to  
80 each emission source. In contrast, *top-down* methods (or inverse modeling), in which observed mixing ratios are  
partitioned into their sources, have also been used for constraining or cross-checking bottom-up emissions (Huo et  
al., 2009; Zhang et al., 2009; Cohen and Wang, 2014; Fischer et al., 2016; Miller and Michalak, 2017).

Efforts to understand urban-scale emission using direct observation have been undertaken in several large  
cities including the Northeastern U.S. (Boston, Baltimore/Washington D.C., He et al., 2013; Dickerson et al., 2016),  
85 the U.S. Mountain West (Salt Lake City, Strong et al., 2011), Indianapolis (Mays et al. 2009; Turnbull et al., 2015;  
Lamb et al., 2016; Lauvaux et al., 2016), and the Southwestern U.S., especially the Los Angeles basin (Duren et al.,  
2011; Kort et al., 2012). There are several methods to quantify emissions: in-situ measurements and flask collection  
through surface tower systems, space-based satellite retrieval, airborne in-situ measurements, mesoscale models, and  
Large Eddy Simulation (LES) modeling. As part of the Indianapolis Flux Experiment (INFLUX) project, airborne  
90 and tower measurements have been collected throughout Indianapolis to generate an extensive database. Over the  
western U.S., a legacy dataset over Salt Lake City has collected measurements of CO<sub>2</sub> using surface tower systems  
for more than one decade (Pataki et al., 2005, 2007; Strong et al., 2011). Results from this extensive dataset have  
included seasonal variability over years and source apportionment into anthropogenic and biogenic sources. While  
those efforts reach general agreement on emission inventories across the cities, they have limitations due to their  
95 geographical differences in topography, climatology, different source attributions (such as types of industry and  
agriculture), as well as differences in the measurement and analysis methods.

One approach for estimating CO<sub>2</sub> and CH<sub>4</sub> fluxes over cities is the use of an aircraft-based mass balance  
method. Several studies have demonstrated the utility of this approach (Kalthoff et al., 2002; Mays et al., 2009;  
Turnbull et al., 2011; Karion et al., 2013, 2015; Cambaliza et al. 2014; Gordon et al., 2015; Tadić et al., 2017). Mass



100 balance methods utilize many length scales and patterns. The flights target mostly local scales (< 3 km) and areas  
around the point sources (Nathan et al., 2015; Conley et al., 2017), but they also characterize urban-scales (e.g. 25 x  
10 km for Gordon et al. (2015), 4 x 9 km for Tadić et al. (2017)) and the large-scale (40 km up to 175 km, especially  
for a downwind curtain flight (Mays et al., 2009; Turnbull et al., 2011; Karion et al., 2015)).

The flight patterns can be classified into three different categories: 1) single-height transect flight, 2) single  
105 screen ("curtain") flight with multiple transects, and 3) enclosed shapes (box, cylinder) (see Fig. S1 in  
Supplementary Appendix). Commonly, there are assumptions made in these airborne sampling approaches. First, the  
single-height transect approach assumes a well-mixed boundary layer. Karion et al. (2013) measured CO<sub>2</sub> and CH<sub>4</sub>  
along a single-height transect with an assumption of uniform vertical mixing. Turnbull et al. (2011) performed a flux  
estimate by incorporating detailed meteorological information and transecting an emission plume with an aircraft.  
110 These studies also assumed that emissions originate from point sources such as pipes and smokestacks, and travel  
downwind so that all pollution is reflected on the downwind "curtain" with constant wind speed. Second, the single-  
screen multi-transect method does not assume a uniformly mixed boundary layer condition but is dependent upon a  
constant wind speed. Without a well-mixed boundary layer assumption, Cambaliza et al. (2014) measured CH<sub>4</sub>  
along multiple height transects downwind of the city of Indianapolis (See Fig. S1a in Supplementary Material).  
115 However, they assumed that winds at the time of measurement were the same as at the time of emission (i.e., winds  
after the methane release were time-invariant). Third, the enclosed 3-D shape flights do not presuppose any of the  
assumptions described above. Gordon et al. (2015) measured various GHG with a stacked box flight pattern, to  
capture the vertical variation in mixing ratio both upwind and downwind. Tadić et al. (2017) and Conley et al.  
(2017) accomplished emission estimates by flying a cylinder pattern near an emission source to measure GHG both  
120 upwind and downwind for analysis based on the divergence theorem. More recently, Baray et al. (2017) used both a  
screen flight and box flight approach around oil sands facilities and showed that each flight pattern could be  
preferred, depending on the types of emissions and spatial characteristics.

While these assumptions may be valid in certain conditions, they do not always hold. Most cities include  
multiple sectors, including industry, agriculture, and residential areas, and can have daily variability in wind that  
125 influences flux patterns. For example, a local landfill, various highways and several airports around Sacramento are  
significant sources of emissions and of uncertainty. To minimize uncertainty in flux estimates, these sources must be  
taken into consideration. The method of extrapolation to unsampled areas can also be a large source of uncertainty.  
For example, Gordon et al. (2015) demonstrated the significant impact of extrapolation methods over the unsampled,  
near-surface region on the final emission estimate, unlike Cambaliza et al. (2014) who assumed that the city plume  
130 is rarely observed in a transect between the surface and the lowest altitude flight measurement. Assumptions can  
break down when wind direction and speed vary with time and three dimensional space (e.g. longitude, latitude and  
altitude; see Fig. 2S); incorrect use of wind data can result in increased uncertainty and reduction of accuracy. Flux  
estimates also require an estimate of the planetary boundary layer height (PBLH), an important physical parameter  
that is hard to measure. State-of-the-art atmospheric models and reanalysis products often estimate the PBLH, but  
135 substantial differences have been observed in existing models and reanalysis data (Wang et al. 2014). In addition,  
entrainment from the free troposphere into the planetary boundary layer (PBL) and fluxes from the surface have



been ignored in most previous studies. Thus, more careful consideration and understanding of these factors are required for determining emission estimates using any of the three mass balance flight patterns.

The primary goals of this study are: i) to design and execute the cylindrical flight patterns for greenhouse gas observations for an urban domains (Fig. S1b in Supplementary Material) and to assess the impact of different interpolation and extrapolation methods on the emission estimate, ii) to test the sensitivity of emission estimates to a variety of factors such as wind, background mixing ratios, and different flux estimation methods, and finally iii) to examine the importance of vertical mass transfer on the flux estimates. To address these goals, we collect CO<sub>2</sub> and CH<sub>4</sub> data during three flights over Sacramento (See Fig. S3 in Supplementary Material) for urban (35–60 km) and local scales (< 3 km), and determine emission fluxes using various treatments of wind conditions, background value, and vertical mass transfer. The data and methodology are presented in section 2. Kriging results for the CO<sub>2</sub> and CH<sub>4</sub> concentrations fluxes for all three flights are shown in section 3. The sensitivities of flux estimates to different use of the wind, background value, and vertical mass transfer are also investigated. The conclusions of this study are presented in section 4.

## 2. Data and Methods

### 2.1 Data Collection

In situ measurements of CO<sub>2</sub> and CH<sub>4</sub> were performed as part of the Alpha Jet Atmospheric eXperiment (AJAX) project. The CO<sub>2</sub> and CH<sub>4</sub> instrument (Picarro Inc., model 2301-m) is calibrated before each flight using whole-air standards from the National Oceanic and Atmospheric Administration's Earth System Research Laboratory (NOAA/ESRL). Water vapor corrections using Chen et al. (2010) were applied to calculate the dry mixing ratios of CO<sub>2</sub> used during this study. The overall uncertainty was determined to be 0.16 ppm for CO<sub>2</sub> and 2.2 ppb for CH<sub>4</sub> (Tanaka et al., 2016; Tadić et al., 2014).

The Meteorological Measurement System (MMS) measures high-resolution pressure, temperature, and 3-D ( $u$ ,  $v$ , and  $w$ ) winds (Hamill et al., 2016). Take off time from Moffett Field was between 20:30 and 21:00 UTC for each flight day discussed here. For the November flights, local time was 13:30–14:00 Pacific Standard Time; for the July flight, take off was at 12:37 Pacific Daylight Time.

### 2.2 Extrapolation to the Surface

Because the lowest flight path was typically 250–380 m above the surface and there were no ground-based measurements along the flight tracks, there is always a gap in measurement data between the surface and the lowest flight altitude. Many studies adopt a well-mixed layer assumption below the lowest flight altitude (Karion et al., 2013), but these unmeasured values can lead to a significant bias and large uncertainties in estimating GHG mixing ratios and fluxes, depending on interpolation and extrapolation schemes (Gordon et al., 2015). Thus, we investigated four methods to extrapolate mixing ratio values to the surface, which are termed 1) constant, 2) exponential fit, 3) Gaussian fit, and 4) kriged fit. The constant method assumes an elevated plume with a constant background level. The background level is derived from the lowest flight measurement:  $X(t, z) = X(t, z_L)$  for  $z_0 < z < z_L$ , where  $z_L$  is the lowest flight level. The exponential-fit method assumes an exponential decay of  $X(t, z)$  from  $z_L$  to  $z_0$ . The



detailed method is based on Gordon et al. (2015). The Gaussian fit method is similar to exponential fit method, except that the surface-sourced plume dispersion follows a Gaussian distribution. The kriged fit was applied down to the surface level, extended from the sampled area above.

### 175 2.3 Elliptical Fit and Kriging

Because the aircraft flew in a cylindrical pattern around the city, the flight paths were transformed into a polar coordinate system. The path was projected to the surface first and fit into an ellipse using least squares method to minimize the difference between the measured data and the fitted data. Then, we computed each point using the major and minor axis of the ellipse and parameter  $t$ . Each point on the ellipse was represented by a single parameter ( $t$ , eccentric anomaly), according to the equations:

$$\begin{aligned} X(t) &= X_0 + a \cos t \cos \phi - b \sin t \sin \phi \\ Y(t) &= Y_0 + a \cos t \sin \phi + b \sin t \cos \phi \end{aligned} \quad (1)$$

where  $a$  and  $b$  is a radius of the major, minor axis of the ellipse, respectively,  $\phi$  is the angle between the X-axis and the major axis of the ellipse, and the parameter  $t$  is obtained from Eqn. (1), varying from 0 to  $2\pi$ . Then, the data was gridded into a two-dimensional plane [ $t$ , height].

In order to assess the strengths of a kriging approach to quantifying emissions, two interpolation methods were assessed: interpolation using kriging and that using an exponential weighting function. The exponential weighting function at a given point ( $P$ ) was defined as the weighted average of all the other points where the weights decrease exponentially with distance to  $P$ . Both approaches captured the general plume pattern (regions with high and low concentrations of  $\text{CO}_2$ ), but the kriging approach did better at capturing individual plume features such as the range and magnitude, while interpolation with the exponential weighting function could not resolve such details (see Fig. S4 in Supplementary Material). Another benefit of kriging is that it can estimate values at unsampled locations using a weighted average of neighboring samples, thus reproducing the characteristics of the observed values.

Interpolation was performed by the ordinary kriging method (Chilés and Delfiner, 2012), modified from the IDL v8.1 kriging tool to fit an elliptical pattern. We chose ordinary kriging because there is no obvious trend in the data we use. Before kriging, we modeled the variograms for all relevant variables. A variogram (or semivariogram) is a function describing the degree to which the data are correlated as a function of the separation distance between observations. The empirical semivariogram of the data was fit using an exponential variogram model, based upon visual inspection of the experimental variograms. Three parameters were used to fit the theoretical variogram, namely the sill (the expected value of the semivariance between two observations as the lag distance goes to infinity), the range (the distance at which the variogram reaches approximately 95% of the sill), and nugget (representative of measurement error and amount of microscale variability in the data). Variogram modeling was first performed to derive parameters required to obtain ordinary kriged estimates. Various other types of kriging exist in the literature on quantifying greenhouse fluxes (Tadić et al., 2017), but examining their differences is beyond the scope of this study.



We kriged the CO<sub>2</sub>, CH<sub>4</sub>, wind, temperature, and pressure observations to obtain both the estimate and the uncertainty for each variable at each grid point. The individual semivariograms of the variables for each flight were produced, and we present them for one flight in Fig. S5 in Supplementary Material. For each flight, the sampled data  
210 were kriged to a grid of maximum height divided by 150 in the vertical dimension; the horizontal dimension was kriged from end to end of the flight transect, enclosing the circumference of the entire city, divided by 360 in the horizontal direction. The vertical dimension was interpolated from the ground to the top of the flight measurement, but only data up to the estimated planetary boundary layer height (PBLH) was used for computing the flux estimates.

The uncertainty in the kriged results was assessed using the variance (and the standard deviation) of the kriged  
215 estimate at each point, as in Mays et al. (2009) and Nathan et al. (2015). In a statistical sense, the interpolated downwind CO<sub>2</sub> and CH<sub>4</sub> concentration is one of the largest sources of uncertainty in flux error estimates because the downwind flux calculation requires interpolated values at unsampled locations. Another well-known significant source of uncertainty comes from the wind measurement (Mays et al., 2009; Karion et al., 2015; Tadić et al., 2017). The grid resolution can also be a source of uncertainty. Nathan et al. (2015) reported that changing the grid  
220 resolution by a factor of 2 in either direction resulted in a 4 % absolute change in the emission rate, and showed that the grid size does not significantly bias the interpolated emission rates for their study. However, emission estimates may depend on scales of variability in the measured quantities and the grid resolution, in that the grid resolution has to be sufficiently fine to capture the observed scales of variability. They also demonstrated that the selection of the variogram model they used, such as Gaussian-cosine, linear, exponential, and exponential-bessel variogram, did not  
225 affect the final emission estimate substantially (the difference is less than 5 %) in their case study. Moreover, uncertainties in greenhouse gas mixing ratio measurements, as well as in wind speed and direction, directly propagate the emission rates uncertainties.

#### 2.4 Treatment of Measured Wind

To test the sensitivity of fluxes to the choice of the background value and the wind characteristics, we applied  
230 the measured high-resolution (1 Hz) in-situ wind data to the flux calculation in two different ways. In one we used the measured wind at specific measured points without any correction (hereafter we refer to it as “raw wind”). In this case, inflow and outflow are not balanced within a cylinder. Alternatively, we averaged horizontal wind at each vertical level, so that air (mass) coming into the cylinder equaled air leaving the cylinder. By assuming non-divergence, mass can be balanced (here we refer to it as “mass-balanced mean wind”).

#### 235 2.5 Planetary Boundary Layer Height (PBLH) and Entrainment

The potential temperature profile, which indicates atmospheric static stability and which significantly affects pollutant diffusion, is the most common operational method to determine PBLH. We determined PBLH as the altitude of the maximum gradient from a vertical profile of potential temperature (Wang et al., 2008) obtained from the MMS measurements. No significant sensitivity was found using several different PBLH detection algorithms,  
240 such as the parcel method (the interaction between dry adiabatic lapse rate and temperature), rapid decrease in water



vapor (Wang and Wang, 2014), or Richardson number method (Wang et al. 2008). A simple example is shown in Supplementary Material Fig. S6.

245 The boundary layer growth is determined by the sum of entrainment velocity ( $w'$ ) and large-scale mean vertical velocity (Vilà-Gueru de Arellano et al. 2004, Faloona et al., 2005, Trousdell et al., 2016). Here we define the entrainment (surface) flux as the turbulent flux of the scalar at the boundary layer height (surface). Then we compute the entrainment flux at the top of the cylinder by multiplying the area of the top of the cylinder with  $E = \overline{(w'c')}_h \cdot A$  where  $A$  is the area of the top of the cylinder,  $c' = (C(t, z) - C_{bg}(h))$ ,  $C(t, z)$  is the CO<sub>2</sub> mass (g m<sup>-3</sup>) at a given point surrounding the top of the cylinder at  $z=h$ , and  $C_{bg}(h)$  is the background concentration of CO<sub>2</sub> at the top of the boundary layer. The CO<sub>2</sub> mass is calculated from the CO<sub>2</sub> mixing ratio (ppmv).  
250 Using this, we could make direct observations of the entrainment flux by measuring vertical velocity together with the trace gas mixing ratio throughout the boundary layer. The surface flux is computed at the surface ( $z = 0$ ) in a similar manner.

## 2.6 Background Values, Flux Calculation and Emission Rate

Figure 1 shows a map of the AJAX flight tracks over Sacramento and the vertical structure of the CO<sub>2</sub> mixing ratio on November 17, 2015. A simple illustration of the air flow (computed as the pressure divided by the magnitude of the wind vector normal to the cylindrical surface) demonstrates the basic idea of this study, Gauss's divergence theorem, which relates the flow through the surface to the flow inside the surface. Mass coming in and out of the cylinder should be conserved if there is no leak throughout the top and the bottom of the cylinder (i.e., the flow into the cylinder balances with the flow out of the cylinder). More precisely, the outward flux of a vector through a closed system is equal to the volume integral of the divergence over the region inside the surface. Since the atmosphere has no upper boundary, we assume that vertical mass transfer is accomplished through an entrainment from the top of the PBL, and surface flux from the bottom of the cylinder near the surface. In this way, the oval cylinder we design over the city has a closed surface, and the flux inside the cylinder is equal to the sum of the emission flux at the bottom.  
260

265 Background values are one of the most important factors in obtaining flux estimates. Here we used three distinct methods to determine background values and calculate emission fluxes for each gas. First, we used the *minimum* value at each vertical level of the data (i.e., from the surface to the top of the PBL). Second, we used the *average* value at each vertical level. Third, we used two different vertically invariant, constant values throughout the whole height from the surface to the top of the PBL.

270 We determined kriged data for each field from the measured CO<sub>2</sub>, CH<sub>4</sub>, wind, temperature, and pressure, and then estimated the local background concentrations for both trace gases following three different approaches described above. Then we subtracted these background values from the trace gas data at each grid point. To convert the volume mixing ratio [ppmv] to a mass concentration [g m<sup>-3</sup>], the number of CO<sub>2</sub> or CH<sub>4</sub> molecules were computed based on the ideal gas law using the kriged temperature and pressure. Then, the net mass flow [g m<sup>-2</sup> s<sup>-1</sup>] was integrated in the horizontal and vertical directions from the surface up to the top of the cylinder.  
275



$$F = \iint \bar{U}(\theta, z) \sin(\alpha) \cdot (C(\theta, z) - C_{bg}) L d\theta dz \quad (2)$$

where  $L$  is the difference between two points on the ellipse,  $\bar{U}(\theta, z)$  is the wind speed,  $\alpha$  is the angle of the wind velocity relative to the flux surface,  $C$  is the concentration ( $\text{g m}^{-3}$ ), and  $C_{bg}$  is the background concentration at each level  $z$ . The component of the wind perpendicular to the flux surface was used in the flux calculation.

### 3. Results

#### 3.1 Dependence of GHG mixing ratios on different interpolation schemes and extrapolation fits

Estimates of GHG mixing ratios along the cylindrical boundary of the flight pattern are sensitive to the choice of interpolation schemes and extrapolation fits, especially at lower altitudes where there are no aircraft data available. Figure 2 shows  $\text{CO}_2$  and  $\text{CH}_4$  mixing ratios for November 18, 2013 and November 17, 2015 at several locations over Sacramento. These results demonstrate that a large source of uncertainty and difference comes from not only the interpolation but also the extrapolation of the data between the lowest flight level and the surface. For example, uncertainty in estimated GHG mixing ratios below the lowest flight level (indicated by the yellow diamond) can be large (up to  $\sim 20\%$ ). In the worst cases,  $\text{CO}_2$  mixing ratios span more than 60 ppm at the surface among the methods;  $\text{CH}_4$  ranges  $> 0.15$  ppm. Note that the differences between interpolation schemes where data exists (above  $\sim 250\text{--}380$  m) were smaller than the differences between the values obtained from the various methods below the lowest flight data. Without ground-based data, a proper choice of extrapolation schemes requires knowledge or presumption of the mixing ratio behavior in this region. Gordon et al. (2015) proposed that the case of elevated sources beneath the lowest flight level is best suited to constant extrapolation of mixing ratio to the surface (blue curve), while a ground-source concentration should be represented with an exponential-fit extrapolation (red).

The various fits rely on different assumptions; the ordinary kriging method (magenta traces in Figure 2) also requires some assumptions (e.g., constant mean, constant variance, second-order stationarity and isotropy, and validity of the theoretical model). Ordinary kriging leverages spatial and statistical properties of the observations to derive estimates, and seems to be less arbitrary than alternative interpolation/extrapolation methods. We note the similarity between the kriged values and the constant extrapolation method for both  $\text{CO}_2$  and  $\text{CH}_4$ .

#### 3.2 Observed and Kriged GHG Mixing Ratios

Figure 3 shows the measured methane over Sacramento, CA, for November 18, 2013, and the projection to the ground (plan-view), the grid in panel (d) shows how we fit the data to compute the “flux surface” using kriging. The kriged  $\text{CH}_4$  not only captures the measured  $\text{CH}_4$  mixing ratio, but also fills the gap of the unsampled area based on the observed data characteristics. Maximum values were found at  $38.73^\circ$  N,  $121.2^\circ$  W to  $38.68^\circ$  N,  $121.45^\circ$  W at 300 m. The high  $\text{CH}_4$  region corresponds with highways, airports and dairy farms, especially near the surface. Compared to the conventional interpolation without considering the individual characteristics of data, kriging can capture the most important features of the data (see Fig. S4 in Supplementary Material).



Figure 4 shows the observed and kriged CO<sub>2</sub> mixing ratio, and kriging uncertainty at each grid point on  
310 November 18, 2013, and November 17, 2015. The kriged CO<sub>2</sub> fields capture the main features of the observed CO<sub>2</sub>  
plume well. The centers of the large CO<sub>2</sub> plumes differed somewhat in magnitude and width, reflecting the varied  
source characteristics for CO<sub>2</sub>. The CO<sub>2</sub> mixing ratios on November 18, 2013, were much larger (up to 25 ppm  
higher at most spots) than those on November 17, 2015.

The observations in Figs. 4(a–f) suggest that the vast majority of the emission sampled by the flights originates  
315 in the region identified as traffic regions (Roseville), airports, metropolitan areas (Arden-Arcade-Roseville, Fair  
Oaks, North Highland), and dairy farms. On both days, the largest CO<sub>2</sub> mixing ratios were seen on the northeast side  
of the oval, which was the downwind side when sampled in 2013 and the upwind side in 2015 (see Fig. S2 in  
Supplementary Material), indicating that all areas need to be taken into consideration to understand the emission  
characteristics, obtain the actual flux estimates, and reduce uncertainties. The detailed wind direction speed are  
320 shown in Fig. S2 in Supplementary Material.

The vertical stretching pattern of CO<sub>2</sub> mixing ratios in Figs. 4(g–j) appears to be due to the large scale  
difference between the horizontal length (> 120 km) and the vertical length (< 1 km). When we applied our method  
to the local scale (horizontal scale < 3 km, see Fig. 6), or took a small horizontal portion of the large loop (see Fig.  
S4 in Supplementary Material), the vertical stretch pattern disappeared.

Panels (i, j) show the uncertainty was largest near the ground, in particular over the unmeasured area (e.g.,  
325 November 17, 2015, below ~ 200 m, 38.63° N, 121.11° W ~ 38.81° N, 121.18° W), and when the data were observed  
a farther from the elliptical path. The uncertainty in a narrow region at ~1 km for November 17, 2015, resulted from  
the lack of data when aircraft was entering and exiting the cylinder. Furthermore, there were no measurements on  
the ground, so the estimates below 200 m were dependent only on the data around 200 m, which was an additional  
330 source of the uncertainty. Uncertainties of CO<sub>2</sub> were large near the surface, small from 200–900 m, and grew larger  
near the top of the sampled domain.

By assuming that the errors of each factor are Gaussian in nature and each measurement (e.g. CO<sub>2</sub> and wind) is  
independent (no covariance), we estimate the overall uncertainties in the calculated flux by adding the fractional  
uncertainties of the kriged CO<sub>2</sub>, CH<sub>4</sub>, and winds in quadrature, as in Nathan et al. (2015). The overall uncertainties  
335 of the CO<sub>2</sub> and CH<sub>4</sub> mixing ratios (emission estimates) are similar: both of them are less than 2(1) %. When we only  
compute the fluxes for the lateral part of the cylinder using the errors from the CO<sub>2</sub> and CH<sub>4</sub> mixing ratios and the  
wind measurement (normal component of the flux surface), the overall uncertainty of the emission estimate over the  
urban scales is about 4%, and 14% for both CO<sub>2</sub> and CH<sub>4</sub> on November 18, 2013 and November 17, 2015. The  
uncertainties over the local scales over landfill and rice field for both CO<sub>2</sub> and CH<sub>4</sub> on July 29, 2015 are about 35%  
340 and 17%. When we include the entrainment flux at the top and the surface flux at the bottom of the cylinder in  
addition to the flux in the lateral part, the total uncertainty was increased by about less than 1% or remains the same  
for both CO<sub>2</sub> and CH<sub>4</sub>. This appears to be because the contribution of the vertical mass transfer through entrainment  
and the surface flux to the total flux estimates is relatively small, as we will show in section 3.5.

Although we used much more accurate in-situ wind measurements than most past studies for flux calculation,  
345 the wind was still the most important variable for the uncertainty of flux estimates, consistent with previous studies.



This probably partially stems from the uncertainty in the wind at interpolated locations or the sparsity of the measurements. Cambaliza et al. (2014) estimated the uncertainty of the emission rates from kriging analysis is about 50 %. Nathan et al. (2015) also estimated the overall statistical uncertainty of the emission rate over a compressor station in the Barnett Shale as  $\pm 55\%$ . We did not consider the uncertainty of PBLH here because we used the  
350 PBLH based on our in-situ meteorological data and estimate its uncertainty to be  $< 1\%$ .

### 3.3 Sensitivity of Calculated Flux to Wind Treatment

Wind variability and measurement assumptions can lead to errors in the  $\text{CO}_2$  and  $\text{CH}_4$  flux estimates (Mays et al., 2009; Cambaliza et al., 2014, 2015; Nathan et al., 2015; Karion et al., 2013, 2015), and the way in which winds are estimated and quantified especially matters. For November 18, 2013, the wind was southwesterly at the low  
355 altitude, but it changed its direction to southeasterly as height increased. Figure 5 demonstrates the clear difference in flux estimates when the 2-D raw wind and the mean for each level (mass balanced) wind are used. Note that we captured high fluxes (panel f) along with high  $\text{CO}_2$  and  $\text{CH}_4$  mixing ratio when we used the mass-balanced wind (e), while we were less likely to obtain a strong emission signal when using the raw wind data (h), which might be attributed to an imbalance of inflow and outflow to the cylinder. The total flux was  $\sim 7$  times different between wind  
360 cases:  $3.68 \text{ Mt CO}_2 \text{ yr}^{-1}$  and  $13.00 \text{ Gg CH}_4 \text{ yr}^{-1}$  calculated with raw wind, and  $26.55 \text{ Mt CO}_2 \text{ yr}^{-1}$  and  $88.82 \text{ Gg CH}_4 \text{ yr}^{-1}$  with mean wind using the minimum mixing ratio of each level as the background and including vertical mass transfer (see Table 1, rows 1 and 3). The difference was much less for the flight in November 2015.

The importance of wind data on the flux calculation is also seen in local-scale emission calculations (see Fig. S8 in Supplementary Material). For the small cylinder over the landfill site on July 29, 2015, Fig. 6 shows the  
365 observed and kriged  $\text{CH}_4$  mixing ratio and the flux estimation using either the raw wind (c) or the mass-balanced wind (d). As before, the kriged  $\text{CH}_4$  is a good representation of the local characteristics of the  $\text{CH}_4$  field. Reassuringly, the elevated  $\text{CH}_4$  concentration was reconstructed over  $121.19^\circ \text{ W}$ ,  $38.52^\circ \text{ N}$ , which was the actual location of the landfill (See also Fig. S8 in Supplementary Material). The  $\text{CH}_4$  fluxes ( $7 - 10 \text{ Gg CH}_4 \text{ yr}^{-1}$ ) estimated using measured wind (varying with time and space) reflect the strong enhancement of  $\text{CH}_4$  mixing ratios at local  
370 scales. Considering light wind conditions ( $< 2.5 \text{ m s}^{-1}$ ) and high temperature during July, the local emissions are attributed to these high flux estimates. The choice of distinct wind treatments led to a 30% difference in the total  $\text{CH}_4$  estimate and 70% in  $\text{CO}_2$  for this particular case. The  $\text{CH}_4$  concentration and its flux is low over the rice field on that day (See in Fig. S7-S8 in Supplementary Material).

Many previous studies estimated  $\text{CO}_2$  and  $\text{CH}_4$  fluxes based on the mean wind vector at the dominant wind  
375 direction (positive and one direction) and speed (Turnbull et al. 2011; Karion et al. 2015), often using simulated wind obtained from a coarse resolution model. The mass-balanced area-mean wind of the cylindrical loops in this study was based on actual measurements, not coarse resolution model data, which enhances the accuracy of our flux estimates.



### 3.4 Sensitivity to the Choice of Background Concentrations

380 Since both CO<sub>2</sub> and CH<sub>4</sub> mixing ratios vary with altitude, we employed a vertically variant background value  
for each trace gas. Tables 1 and 2 show the calculated CO<sub>2</sub> and CH<sub>4</sub> emission fluxes using two different wind  
methods and two different background treatments for different flight days. The rows labeled "min" were generated  
using the minimum kriged mixing ratio in each altitude band as the background for all data at that level. The rows in  
Table 1 identified by "Bg=avg" used the average mixing ratio on each of the 150 vertical levels as the background  
385 on that level.

The sensitivity of calculated flux to the choice of the background treatment was significant when we used raw  
wind (top two rows in Tables 1). This was true both with vertical mass transfer (Table 1) and without (not shown).  
In contrast, when we use the mean wind, the emission estimates for both CO<sub>2</sub> and CH<sub>4</sub> are nearly identical for either  
choice of the background treatment.

390 Interestingly, emission rate estimates were similar for the case of raw wind with averaged CO<sub>2</sub> or CH<sub>4</sub> as the  
background values and both cases using mass-balanced (mean) wind. To satisfy mass conservation, we also  
computed the entrainment flux from the top ( $z=h$ ) and the surface flux from the bottom of the cylinder ( $z=0$ ). The  
data from Table 1 is also shown in Figure 7 as the non-hatched bars.

Our city-wide estimate of 15-28 Mt CO<sub>2</sub> yr<sup>-1</sup> is higher than the result by Turnbull et al. (2011), who reported  
395 3.5 Mt CO<sub>2</sub> yr<sup>-1</sup> over Sacramento in February 2009. When we examine only the small portion of the ellipse which  
shows the highest CO<sub>2</sub> mixing ratio (e.g. 121.45–121.20° W and 38.65–38.76° N in 2013), CO<sub>2</sub> fluxes calculated  
using spatially varying wind with minimum values for background were 4.2 Mt yr<sup>-1</sup> in 2013 and 5.5 Mt yr<sup>-1</sup> in 2015.  
When calculating fluxes using mean wind with average values for background, the "downwind side" emission rates  
were about 4.4 and 3.5 Mt yr<sup>-1</sup>. From this study, the fluxes from the downwind portion of the cylinder were  
400 responsible for only ~15–23 % of the total emissions.

Our city-wide estimate of 89-95 Gg CH<sub>4</sub> yr<sup>-1</sup> on November 18, 2013 corresponds to 53-57% of the 167 Gg CH<sub>4</sub>  
yr<sup>-1</sup> (about 140–220 Gg yr<sup>-1</sup>), reported by Jeong et al. (2016) over Region-3 (San Joaquin Valley area including  
Sacramento). On November 17, 2015, we calculate a significantly smaller emission rate (8 – 11 Gg yr<sup>-1</sup>). Direct  
comparison between different flux estimates is challenging due to various factors, such as i) differences in the areas  
405 covered, ii) differences between bottom-up inventory and top-down estimates, iii) the variance of measurement  
methods (tower, aircraft, and model), iv) underestimation of the emissions from known sources, v) seasonal and  
interannual variability, vi) different spatial coverages, and vii) lack of understanding of unidentified sources. This  
will be one of the most important areas for improvement for establishing better emission estimate databases in the  
future.

### 410 3.5 Importance of Including Vertical Mass Transfer

Many previous studies assume that vertical mass transfer can be neglected (Cambaliza et al., 2014; Conley et  
al., 2017). To quantify the validity of this assumption, we compare the flux determined when including or neglecting  
the entrainment and surface fluxes. Figure 7 shows the urban-scale emission rate estimates over Sacramento, CA  
using spatially and temporally varying ("raw") wind and the mean ("mass balanced") wind. We chose the



415 background values as i) average value of each vertical level, ii) the minimum value of each level, or iii) one of two  
fixed values at all altitudes. The fixed values were chosen in the range between the minimum and median mixing  
ratios. Note that the total fluxes using the mean wind were not sensitive to the choice of the background value (<  
3 %, whether background value was minimum, average, or constant values). However, as discussed in Section 3.4,  
the total fluxes using spatially varying wind ( $u$ ,  $v$ ) were sensitive to the choice of the background value on both  
420 flight days for both gases. Like the urban scale analysis, the flux estimates over the landfill and rice field local scale  
cylinders using raw wind with average background were similar to those using mass-balanced mean wind at each  
level with either minimum or average values as background (shown in Table 2). The differences in  $\text{CO}_2$  and  $\text{CH}_4$   
fluxes with and without (hatched bars in Figure 7) vertical mass transfer were determined to be only 16-17% on the  
urban scale and less important for the local emission estimates (< 10 %).

#### 425 4. Conclusions

We have estimated  $\text{CO}_2$  and  $\text{CH}_4$  fluxes over Sacramento, California, on three days using an airborne in-situ  
dataset from the Alpha Jet Atmospheric eXperiment (AJAX) project and have tested the sensitivity of emission  
estimates to a variety of factors. First, we deployed cylindrical flight patterns of two sizes that differ from common  
curtain flights to estimate the total flux at urban and local scales. We also applied a kriging interpolation method to  
430 the data, capturing the characteristics of the data at both observed and unsampled locations. Second, we tested the  
sensitivity of flux estimates to the wind, background concentrations, and different flux calculation methods. We  
found that the way in which winds are estimated and how background values were chosen were the dominant factors  
in determining the total flux estimate. Third, we took into account not only the inflow and the outflow through the  
cylinder around the city, but also the vertical mass transport (e.g., entrainment and surface flux) and tested the  
435 sensitivity of the total flux estimate to the vertical mass transfer for both urban and local scales.

When we used the area-mean wind for flux calculation, the sensitivity of the emission estimate to the choice of  
background was minimal (Table 1). Urban scale  $\text{CO}_2$  flux was similar in both years sampled (20-27 Mt  $\text{CO}_2 \text{ yr}^{-1}$ ),  
but the calculated  $\text{CH}_4$  flux was different by  $\sim 9\times$  ( $\sim 90 \text{ Gg CH}_4 \text{ yr}^{-1}$  in 2013 and  $\sim 10 \text{ Gg CH}_4 \text{ yr}^{-1}$  for the flight in  
2015). Using measured winds, not averaged, produced similar flux estimates when the background mixing ratio was  
440 set to the average value on each vertical layer. In contrast, choosing the background as the minimum value observed  
on each level led to calculated fluxes that were substantially lower for the flight in 2013.

The Planetary Boundary Layer Height (PBLH) was calculated using the vertical profiles of potential  
temperature and was used together with the vertical fluxes for computing the entrainment from the top and the  
surface flux from the bottom of the cylinder. Neglecting vertical mass transfer can increase the uncertainty of the  
445 total flux estimate by up to 17 % in our cases.

The advantage of the closed shape (i.e., elliptical in this study) approach over the curtain flight is to make a  
more precise “total” emissions estimate possible by taking into account all unknown sources of emissions.  
Regarding the balanced incoming and outgoing fluxes within a closed volume, we suggest that emission estimates  
using mean measured wind computed over a closed shape can be beneficial for several reasons. First, the flux  
450 estimates calculated using mass-balanced mean wind reduce the sensitivity to the choice of background. From Fig. 6



and Table 1 we found that the background value is one of the major sources of uncertainty in both CO<sub>2</sub> and CH<sub>4</sub> emission estimates, but when we use as the background value either the minimum value (which is often similar to the air away from the source) or the mean value at each vertical level, the final flux estimates become similar. Second, when we analyze only a small portion of the large loop (e.g., downtown hot spot region) to mimic the curtain flight style, the final flux estimates are highly sensitive to the background choice no matter how the measured wind data are treated. These also indicate that the flux estimates for the closed elliptical loops over the city would reduce sensitivity to the choice of background values.

The local CH<sub>4</sub> flux over a landfill is one-tenth to one-third the total emission flux over Sacramento in wintertime, suggesting a local point source of CH<sub>4</sub> can play a significant role in enhancing overall CH<sub>4</sub> concentrations. In general, CH<sub>4</sub> over a rice field showed lower emission rates than those over the landfill, and this may be due to the relatively high wind, no particular point source, and reduced CH<sub>4</sub> emissions as a result of low humidity (dry) conditions. Considering the wind speed was much lower in July (especially over the landfill), this indicates that most of the emission was produced from local sources for the July 29, 2015, case. On the other hand, the strong winds observed on November 18, 2013 came from the southeast, isolating high concentrations of CO<sub>2</sub> downwind of industrial facilities. On November 17, 2015, stronger upper level wind came from the north, but the weaker lower level wind originated from the south. High concentration of CO<sub>2</sub> at lower altitudes were thus located downwind of a major highway intersection and residential sectors. Elevated CH<sub>4</sub> concentrations were found over local, narrow, and isolated areas for both November flights.

The spatial variation of CO<sub>2</sub> and CH<sub>4</sub> observed in the cylindrical flight pattern measured over Sacramento reveals that there were several local sources throughout the entire city, not only concentrated on the downwind side. Furthermore, variability of wind may contribute to different flux estimates at a similar time of year (e.g., November). Our sensitivity study reveals that the unbalanced wind varying with time and space may be a source of methodological uncertainty. Thus, use of constant wind speed or unrepresentative coarse resolution of wind (e.g., model output with coarse resolution) by focusing only on the downwind side may lead to significant uncertainty in the estimation of the greenhouse gas emission fluxes. The size of the ellipse measuring urban emission appeared to be another factor affecting flux estimates. In general, vertical mass transfer does not significantly contribute to the total emission estimate (especially at local scales), but it can modify total emission estimates by up to 17 % for urban scales in our cases. For the local scale (~ 3 km), vertical mass transfer was not important due to the small turbulent fluxes.

There are still several issues to be addressed further. First, further sector-specific emissions and their uncertainties for CO<sub>2</sub> and CH<sub>4</sub> need to be further identified (Miller and Michalak, 2017). Second, the seasonality of sensitivity of emission estimates to various factors needs to be examined. Finally, understanding the sources of uncertainties in emission estimates, and how different they can be under various conditions need to be investigated further. We found that the uncertainty of the emission estimates can be also sensitive to temperature, and potential temperature (to determine PBLH). In this sense, the changing climate over California makes it harder to predict future emission patterns. The use of aircraft measurements presented here provides the tremendous opportunity to measure the entire urban plume.



490 This effort is not limited to one particular city. There has been increasing interest in performing inter-city  
comparisons to validate datasets in a more efficient and adequate manner, to create a uniform database that is useful  
for emission controls (Urban greenhouse gas measurements workshop, 2016). Given that data are available over  
several cities which have different conditions, we can test how to obtain emission estimates from several cities.  
Differences in the socio-economic, geologic, and industrial characteristics of cities lead to a need to compare  
emission estimates between them, as together they can contribute significantly to the total GHG emission at national  
and global scales. Thorough comparison among datasets and a customized sharing system between different  
495 research groups will lead to reducing the uncertainty of emission estimates.



#### **Author contribution**

500 Ju-Mee Ryoo, Laura T. Iraci, Tomoaki Tanaka, Josette E. Marrero, Emma L. Yates, Warren Gore designed the experiments, and they carried them out. T. Paul Bui and Cecilia S. Chang prepared MMS instruments on Alpha jet and Jonathan. M. Dean-Day processed the data. Anna M. Michalak and Jovan Tadić participated in experiment design and supported the interpretation of the statistical analysis. Inez Fung gave insightful comments, and Laura T. Iraci gave helpful guidance in formulating the structure of this study. Ju-Mee Ryoo developed the statistical model code and performed the analysis as well as prepared the manuscript with contributions from all co-authors.



505 **Competing interests**

The authors declare that they have no conflict of interest.



### Acknowledgements

510       The authors appreciate the support and partnership of H211 L.L.C, with particular thanks to K. Ambrose, R. Simone, T. Grundherr, B. Quiambao, and R. Fisher. Technical contributions from Z. Young, R. Vogler, E. Quigley, and A. Trias made this project possible. Funding was provided by the NASA Postdoctoral Program, Bay Area Environmental Research Institute, and Science and Technology Corporation. Funding for instrumentation and aircraft integration is gratefully acknowledged by Ames Research Center Director's funds. Resources supporting  
515 this work were provided by the NASA High-End Computing (HEC) Program through the NASA Advanced Supercomputing (NAS) Division at NASA Ames Research Center.



## References

- Andres, R.J., Fielding, D.J., Marland, G., Boden, T.A., Kumar, N. and Kearney, A.T.: Carbon dioxide emissions  
520 from fossil-fuel use, 1751-1950, *Tellus*, 51B, 759-765, 1999.
- Andrews, C.: Greenhouse gas emissions along the rural to urban gradient, *J. Environ. Plann. Manage*, 51, 847-870,  
2008.
- Baray, S., Darlington, A., Gordon, M., Hayden, K. L., Leithead, A., Li, S.-M., Liu, P. S. K., Mittermeier, R. L.,  
Moussa, S. G., O'Brien, J., Staebler, R., Wolde, M., Worthy, D., and McLaren, R.: Quantification of Methane  
525 Sources in the Athabasca Oil Sands Region of Alberta by aircraft mass-balance, *Atmos. Chem. Phys. Discuss.*,  
<https://doi.org/10.5194/acp-2017-925>, 2017.
- Boden, T.A., Marland, G., and Andres, R.J.: Global, Regional, and National Fossil-Fuel CO<sub>2</sub> Emissions, Carbon  
Dioxide Information Analysis Center, Oak Ridge National Laboratory, U.S. Department of Energy, Oak Ridge,  
Tenn., U.S.A. doi 10.3334/CDIAC/00001\_V2010, 2010.
- 530 California Air Resources Board: California greenhouse gas emission inventory – 2015 edition, available at:  
<http://www.arb.ca.gov/cc/inventory/data/data.htm>, 2015.
- Cambaliza, M. O. L., Shepson, P. B., Caulton, D. R., Stirm, B., Samarov, D., Gurney, K. R., Turnbull, J., Davis, J. J.,  
Possolo, A., Karion, A., Sweeney, C., Moser, B., Hendricks, A., Lauvaux, T., Mays, K., Whetston, J., Huang,  
J., Razlivanov, I., Miles, N. L., and Richardson, S. J.: Assessment of uncertainties of an aircraft-based mass  
535 balance approach for quantifying urban greenhouse gas emissions, *Atmos. Chem. Phys.*, 14, 9029-9050, 2014,  
doi:10.5194/acp-14-9029-2014, 2014.
- Cambaliza, M. O. L., Shepson, P. B., Bogner, J., Caulton, D. R., Stirm, B., Sweeney, C., Montzka, S. A., Gurney, K.  
R., Spokea, K., Salmon, O. E., Lavoie, T. N., Hendricks, A., Mays, K., Turnbull, J., Miller, B. R., Lauvaux, T.,  
Davis, K., Karion, A., Moser, B., Miller, C., Obermeyer, C., Whetstone, J., Prasad, K., Miles, N., and  
540 Richardson, S.: Quantification and source apportionment of the methane emission flux from the city of  
Indianapolis, *Sci. Anthropol.*, 3: 000037, doi: 10.12952/journal.elementa.000037, 2015.
- Chen, H., Winderlich, J., Gerbig, C., Hofer, A., Rella, C. W., Crosson, E. R., Van Pelt, A. D., Steinbach, J., Kolle,  
O., Beck, V., Daube, B. C., Gottlieb, E. W., Chow, V. Y., Santoni, G. W., and Wofsy, S. C.: High-accuracy  
continuous airborne measurements of greenhouse gases (CO<sub>2</sub> and CH<sub>4</sub>) using the cavity ring-down  
545 spectroscopy (CRDS) technique, *Atmos. Meas. Tech.*, 3, 375-386, 2010.
- Chilés, J. P. and Delfiner, P.: *Geostatistics: Modeling Spatial Uncertainty*, 2nd ed., John Wiley & Sons, Inc.:  
Hoboken, NJ. DOI: 10.1002/9781118136188.ch3, 2012.
- Cohen, J. B., and Wang, C.: Estimating global black carbon emissions using a top-down Kalman Filter approach, *J.*  
*Geophys. Res. Atmos.*, 119, 307-323, doi:10.1002/2013JD019912, 2014.
- 550 Conley, S., I. Faloon, S. Mehrotra, M. Suard, D. H. Lenschow, C. Sweeney, S. Herndon, S. Schwietzke, G. Petron, J.  
Pifer, E. A. Kort, and R. Schnell: Application of Gauss's theorem to quantify localized surface emissions from  
airborne measurements of wind and trace gases, *Atmos. Meas. Tech.*, 10, 3345-3358,  
<https://doi.org/10.5194/amt-10-3345-2017>, 2017.



- Dickerson, R.R., Ren, X., Shepson, P.B., Salmon, O.E., Brown, S.S., Thornton, J.A., Whetstone, J.R., Salawitch, R.J., Sahu, S., Hall, D., Grimes, C., Wong, T.M.: Fluxes of Greenhouse Gases from the Baltimore-Washington Area: Results from WINTER 2015 Aircraft Observations, AGU fall meeting abstract #A14F-04, 2016.
- Duren, R.M., and Miller, C.E.: Towards robust global greenhouse gas monitoring, *J. Greenhouse Gas Meas and Manag.*, 1:2, 80-84. doi:10.1080/20430779.2011.579356, 2011.
- Faloona, I., Lenschow, D. H., Campos, T., Stevens, B., Zanten, M. V., Blomquist, B., Thornton, D., Bandy, A., and Gerber, H.: Observations of entrainment in eastern Pacific marine stratocumulus using three conserved scalars, *J. Atmos. Sci.*, 62, 3268-3285, 2005.
- Fischer, M. L.: Atmospheric Measurement and Inverse modeling to improve GHG emission estimates, Air Resource Board project 11-306, ARB report, 2016.
- Gordon, M., Li, S.-M., Staebler, R., Darlington, A., Hayden, K., O'Brian, J., and Wolde, M.: Determining air pollutant emission rates based on mass balance using airborne measurement data over the Alberta oil sands operations, *Atmos. Meas. Tech.*, 8, 3745-3765, doi:10.5194/amt-8-3745-2015, 2015.
- Grimmond, C. S. B., J. A. Salmond, T. R. Oke, B. Offerle, and A. Lemonsu: Flux and turbulence measurements at a densely built-up site in Marseille: Heat, mass (water and carbon dioxide), and momentum, *J. Geophys. Res.*, 109, D24101, doi:10.1029/2004JD004936, 2004.
- Gurney, K. R., Mendoza, D. L., Zhou, Y., Fischer, M. L., Miller, C. C., S. Geethakumar, and de la Rue Ca, S.: High resolution fossil fuel combustion CO<sub>2</sub> emission fluxes for the United States, *Environ. Sci. Technol.*, 43, 5535–5541, 2009.
- Gurney, K.R., Romero-Lankao, P., Seto, K.C., Hutyrá, L.R., Duren, R., Kennedy, C., Grimm, N.B., Ehleringer, J.R., Marcotullio, P., Hughes, S., Pincetl, S., Chester, M.V., Runfola, D.M., Feddema, J.J., and Sperling, J.: Tracking urban emissions on a human scale, *Nature* 525:179-181, 2015.
- Hamill, P., Iraci, L. T., Yates, E. L., Gore, W., Bui, T. P., Tanaka, T., and Loewenstein, M.: A New instrumented Airborne Platform For Atmospheric Research. *Bulletin of the American Meteorological Society*, DOI: <http://dx.doi.org/10.1175/BAMS-D-14-00241.1>, 2016.
- He, H., Stehr, J.W., Hains, J.C., Krask, D.J., Doddridge, B. G., Vinnikov, K.Y., Canty, T.P., Hosley, K.M., Salawitch, R.J., Worden, H.M., and Dickerson, R.R.: Trends in emissions and concentrations of air pollutants in the lower troposphere in the Baltimore/Washington airshed from 1997 to 2011. *Atmos. Chem. Phys.* 13, 1-16, doi:10.5194/acp-13-1-2013, 2013.
- Huo, H., Zhang, Q., He, K., Wang, Q., Yao, Z., and Streets, D. G.: High-resolution vehicular emission inventory using a link-based method: A case study of light-duty vehicles in Beijing, *Environ.Sci. Technol.*, 43, 2394–2399, 2009.
- Idso, C.D., S.B. Idso, R. C. Balling Jr.: The urban CO<sub>2</sub> dome of Phoenix, Arizona. *Physical Geography*, 19, 95–108, 1998.
- Idso, S. B., C. D. Idso, and J. R. C. Balling: Seasonal and diurnal variations of near-surface atmospheric CO<sub>2</sub> concentration within a residential sector of the urban CO<sub>2</sub> dome of Phoenix, AZ, USA, *Atmos. Environ.*, 36, 1655–1660, 2002.



- International Energy Agency: World Energy Outlook 2008, Paris; New Milford, Conn.: International Energy Agency; Turpin Distribution, 2008.
- Jeong, S., et al.: Estimating methane emissions in California's urban and rural regions using multi-tower observations, *J. Geophys. Res. Atmos.*, 121, 13,031–13,049, doi:10.1002/2016JD025404, 2016.
- 595 Kalthoff, N., Corsmeier, U., Schmidt, K., Kottmeier, Ch., Fiedler, F., Habram, M., Slemr, F.: Emissions of the city of Augsburg determined using the mass balance method., *Atmos. Environ.*, 36, Supplement No. 1, S19-S31, 2002.
- Karion, A. et al.: Methane emissions estimate from airborne measurements over a western United States natural gas field, *Geophys. Res. Lett.*, Vol. 40, 1-5, doi:10.1002/grl.50811, 2013.
- 600 Karion, A. et al.: Aircraft-Based Estimate of Total Methane Emissions from the Barnett Shale Region, *Environ. Sci. Technol.* 2015, 49, 8124-8131, DOI: 10.1021/acs.est.5b00217, 2015.
- Kennedy, C. A., et al.: Greenhouse gas emissions from global cities, *Environ. Sci. Technol.*, 43, 7297–7302, 2009.
- Koerner, B., and J. Klopatek: Anthropogenic and natural CO<sub>2</sub> emission sources in an arid urban environment, *Environ. Pollut.*, 116, S45–S51, 2002.
- 605 Kort, E.A., Frankenberg, C., Miller, C.E.: Space-based Observations of Megacity Carbon Dioxide, *Geophys Res Lett* 39, doi:10.1029/2012GL052738, 2012.
- Lamb, B. K., Cambaliza, M.O., Davis, K., Edburg, S., Ferrara, T., Floerchinger, C., Heimbürger, A., Herndon, S., Lavoie, T., Lauvaux, T., Lyon, D., Miles, N., Prasad, K., Richardson, S., Roscioli, J., Salmon, O., Shepson, P., Stirm, B., Whetstone, J.: Direct and indirect measurements and modeling of methane emissions in Indianapolis, IN, *Environ. Sci. Technol.*, 50(16), 8910–8917, doi:10.1021/acs.est.6b01198, 2016.
- 610 Lauvaux, T., Miles, N.L., Deng, A., Richardson, S.J., Cambaliza, M.O., Davis, K.J., Gaudet, B., Gurney, K.R., Huang, J., O'Keefe, D., Song, Y., Karion, A., Oda, T., Patarasuk, R., Sarmiento, D., Shepson, P., Sweeney, C., Turnbull, J., and Wu, K.: High resolution atmospheric inversion of urban CO<sub>2</sub> emissions during the dormant season of the Indianapolis Flux Experiment (INFLUX), *J. Geophys. Res.*, 121, doi:10.1002/2015JD024473, 2016.
- 615 Marland, G., Rotty, R.M., and Treat, N.L.: CO<sub>2</sub> from fossil fuel burning: global distribution of emissions, *Tellus*, 37B, 243-258, 1985.
- Mays, K. L., Shepson, P. B., Stirm, B. H., Karion, A., Sweeney, C., and Gurney, K. R.: Aircraft-based Measurements of the Carbon Footprint of Indianapolis, *Environ. Sci. Technol.*, 43, 7816–7823, 2009.
- 620 Miller, S. M. and Michalak, A. M.: Constraining sector-specific CO<sub>2</sub> and CH<sub>4</sub> emissions in the US, *Atmos. Chem. Phys.*, 17, 3963-3985, doi: 10.5194/acp-17-3963-2017, 2017.
- Nathan, B., Golston, L. M., O'Brien, A. S., Ross, K., Harrison W. A., Tao, L., Lary, D. J., Johnson, D. R. Covington, A. N., Clark, N. N., and Zondlo, M. A.: Near-Field Characterization of Methane Emission Variability from a Compressor Station Using a Model Aircraft, *Environ. Sci. Technol.*, 2015, 7896-7903, DOI: 10.1021/acs.est.5b00705, 2015.
- 625 Oke, T.R.: The energetic basis of the urban heat island. *Q. J. R. Meteorol. Soc.* 108, 1–24, 1982.



- Pataki, D. E., Tyler, B. J., Peterson, R. E., Nair, A. P., Steenburgh, W. J., and Pardyjak, E. R.: Can carbon dioxide be used as a tracer of urban atmospheric transport?, *J. Geophys. Res.*, 110, D15102, doi:10.1029/2004JD005723, 2005.
- 630 Pataki, D. E., Xu, T. Luo, Y. Q., and Ehleringer, J. R.: Inferring biogenic and anthropogenic carbon dioxide sources across an urban to rural gradient, *Oecologia*, 152, 307–322, 2007.
- Rosenzweig, C., Solecki, W., Hammer, A. A., and Mehrotra, S.: Cities lead the way in climate-change action, *Nature*, 467, 909–911, 2010.
- Strong, C., Stwertka, C., Bowling, D. R., Stephens, B. B., and Ehleringer, J. R.: Urban carbon dioxide cycles within the Salt Lake Valley: A multiple-box model validated by observations, *J. Geophys. Res.*, 116, D15307, doi:10.1029/2011JD015693, 2011.
- 635 Tadić, J.M., Loewenstein, M., Frankenberg, C., Butz, A., Roby, M., Iraci, L.T., Yates, E.L., Gore, W., Kuze, A.: A comparison of in-situ aircraft measurements of carbon dioxide and methane to GOSAT data measured over Railroad Valley playa, Nevada, USA. *IEEE Trans. Geosci. Remote Sens.*, 52 (12), <http://dx.doi.org/10.1109/TGRS.2014.2318201>, 2014.
- 640 Tadić, J., Michalak, A., Iraci, L., Ilić, V., Biraud, S., Feldman, D., Thaopaul, B., Johnson, M. S., Loewenstein, M., Jeong, S., Fischer, M., Yates, E., Ryoo, J.-M.: Elliptic cylinder airborne sampling and geostatistical mass balance approach for quantifying local greenhouse gas emissions, *Environ. Sci. Tech*, doi:10.1021/acs.est.7b03100, 2017.
- 645 Tanaka, T., Yates, E. L., Iraci, L. T. Johnson, M. S., Gore, W. Tadic, J. M., Loewenstein, M., Kuze, A., Frankenberg, C., Butz, A., and Yoshida, Y.: Two-Year Comparison of Airborne Measurements of CO<sub>2</sub> and CH<sub>4</sub> with GOSAT at Railroad Valley, Nevada, *IEEE Trans. Geosci. Remote Sens.*, 54 (8), 4367–4375, 2016.
- Trousdell, J.F., S. A. Conley, A. Post, I. C. Faloona, 2016. Observing entrainment mixing, photochemical ozone production, and regional methane emissions by aircraft using a simple mixed-layer model. *Atmos. Chem. Phys. Discuss.*, doi:10.5194/acp-2016-635, 2016.
- 650 Turnbull, J. C., Karion, A., Fischer, M. L., Faloona, I., Guilderson, T., Lehman, S. J., Miller, B.R., Miller, J. B., Montzka, S., Sherwood, T., Saripalli, S., Sweeney, C., and Tan, P.P.: Assessment of fossil fuel carbon dioxide and other anthropogenic trace gas emissions from airborne measurements over Sacramento, California in spring 2009. *Atmos. Chem. Phys.*, 11, 705–721, 2011, doi:10.5194/acp-11-705-2011, 2011.
- 655 Turnbull, J. C., Sweeney, C., Karion, A., Newberger, T., Lehman, S. J., Tans, P. P., Davis, K. J., Lauvaux, T., Miles, N. L., Richardson, S. J., Cambaliza, M. O., Shepson, P. B., Gurney, K., Patarasuk, R., Razlivanov, I.: Toward quantification and source sector identification of fossil fuel CO<sub>2</sub> emissions from an urban area: Results from the influx experiment, *J. Geophys. Res. Atmos.*, 120, 292–312, doi:10.1002/2014JD022555, 2015.
- Urban greenhouse gas measurements workshop: National Institute of Standards and Technology (NIST), Gaithersburg, MD, April 05 – 06, 2016.
- 660 US EPA: Inventory of US greenhouse gas emissions and sinks: 1990–2014, available at: <https://www3.epa.gov/climatechange/ghgemissions/usinventoryreport.html>, 2016.



- Vilà-Gueru de Arellano, J., B. Gioli, F. Miglietta, H. J.J. Jonker, H. K. Baltink, R. W. A. Hutjes, and A. A. M. Holtslag, 2004. Entrainment process of carbon dioxide in the atmospheric boundary layer., *J. Geophys. Res.* 665 109, D18110, doi:10.1029/2004JD004725, 2004.
- Wang, S., Golaz, J.-C., and Wang, Q.: Effect of intense wind shear across the inversion on stratocumulus clouds, *Geophys. Res. Lett.*, 35, L15814, doi:10.1029/2008GL033865, 2008.
- Wang, X., and C. Wang: Estimation of atmospheric mixing layer height from radiosonde data, *Atmos. Meas. Tech.* 7, 1701-1709, doi:10.5194/amt-7-1701-2014, 2014.
- 670 Wofsy, S. C., et al.: Measurement requirements for greenhouse gas concentrations in support of treaty monitoring and verification, *Eos Trans. AGU, Fall Meet. Suppl.*, Abstract GC41G-04, 2010a.
- Wofsy, S. C., McKain, K., Eluszkiewicz, J., Nehr Korn, T., Pataki, D. E., and Ehleringer, J. R.: An observational method for verifying trends in urban CO<sub>2</sub> emissions using continuous measurements and high resolution meteorology, *Eos Trans. AGU, Fall Meet. Suppl.*, Abstract A13F-0280, 2010b.
- 675 Zhang, Q., Streets, D. G., Carmichael, G. R., et al.: Asian emissions in 2006 for the NASA INTEX-B mission, *Atmos. Chem. Phys.*, 9, 5131–5153, 2009.

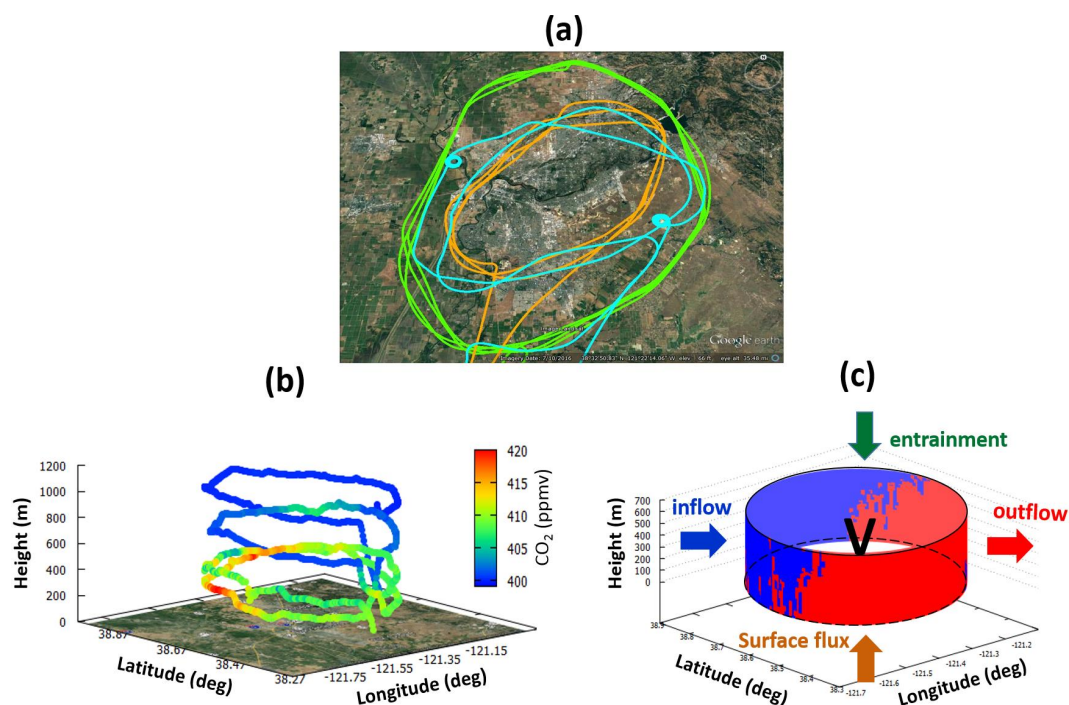


Figure 1: (a) Map of AJAX flight tracks on November 18, 2013 (orange), July 29, 2015 (cyan), and November 17, 2015 (green) plotted in Google™ Earth. (b) Vertical measurements of CO<sub>2</sub> mixing ratio on November 17, 2015, and (c) simple illustration of airflow [ $\text{Kg m}^{-2} \text{s}^{-1}$ ] passing through cylinder (over Sacramento). The shading represents the pressure [hPa =  $\text{Kg m}^{-1} \text{s}^{-2}$ ] divided by the wind vector [ $\text{m s}^{-1}$ ] normal to the cylinder. The blue and red represent inflow and outflow, respectively. The vertical mass transfer through the top and bottom are referred to as the entrainment and surface flux, respectively.

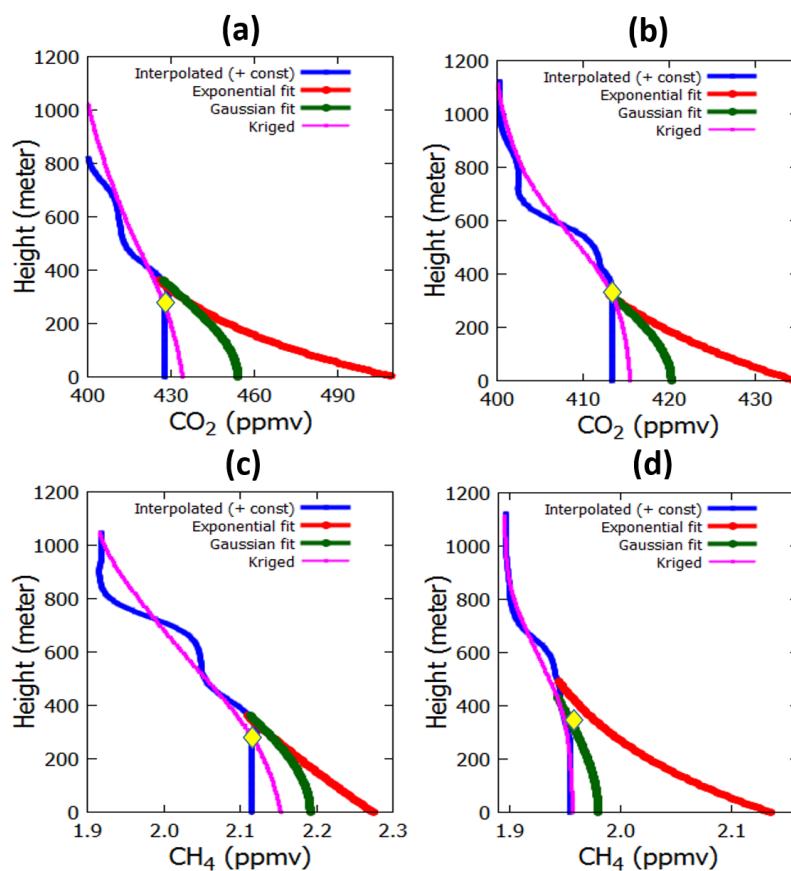
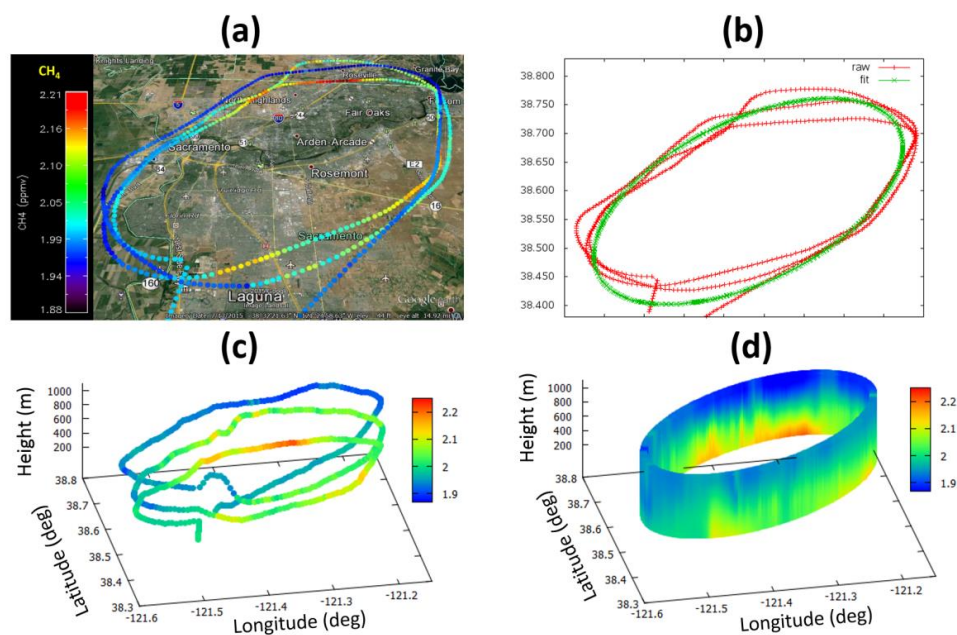
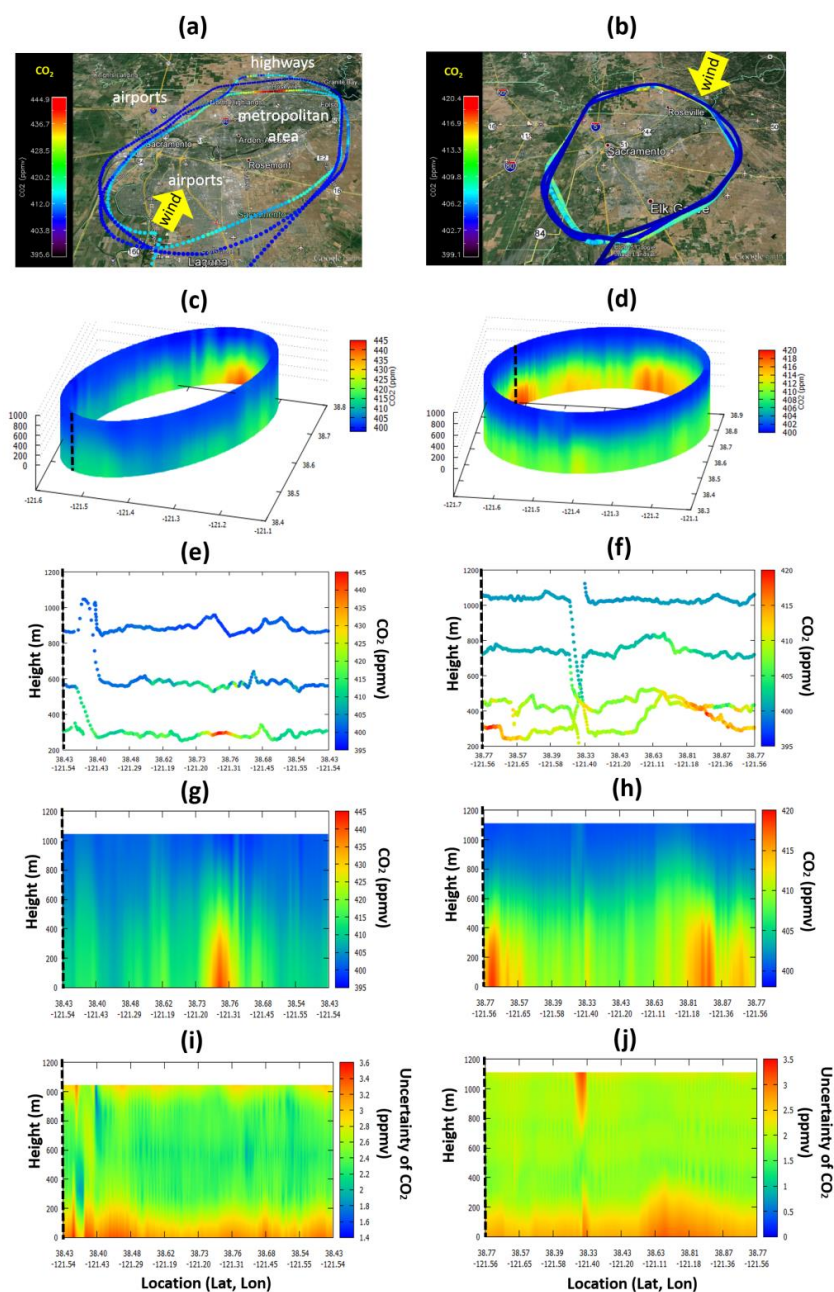


Figure 2: The CO<sub>2</sub> and CH<sub>4</sub> mixing ratios for (a, c) November 18, 2013, around 38.75° N, 121.27° W and for (b, d) November 17, 2015, around 38.84°N 121.27° W for CO<sub>2</sub> and 38.58° N, 121.13° W for CH<sub>4</sub>. The yellow diamond indicates the altitude of the lowest flight data. The kriged values (magenta), interpolated values with exponential weighting function (blue), and extrapolated values using constant (blue line below diamond), gaussian fit (green), and exponential fit (red) are compared. The empirical fits were generated based on the approach by Gordon et al. (2015).



**Figure 3:** (a) Map of AJAX flight tracks colored by CH<sub>4</sub> mixing ratio for November 18, 2013, plotted in Google™ Earth. (b) The data (red) fitted to an oval (green). The observed CH<sub>4</sub> mixing ratios (c) are kriged to generate the cylindrical surface (d). The axes of the oval are approximately 50 and 40 km.



685

Figure 4: (a, b, e, f) Measured CO<sub>2</sub> mixing ratio, (c, d, g, h) the kriged CO<sub>2</sub> mixing ratio, and (i, j) the kriging uncertainty at each grid point on (left) November 18, 2013 and (right) November 17, 2015. The yellow arrows represent the dominant wind directions and the black dashed lines indicate where the surface is split open.

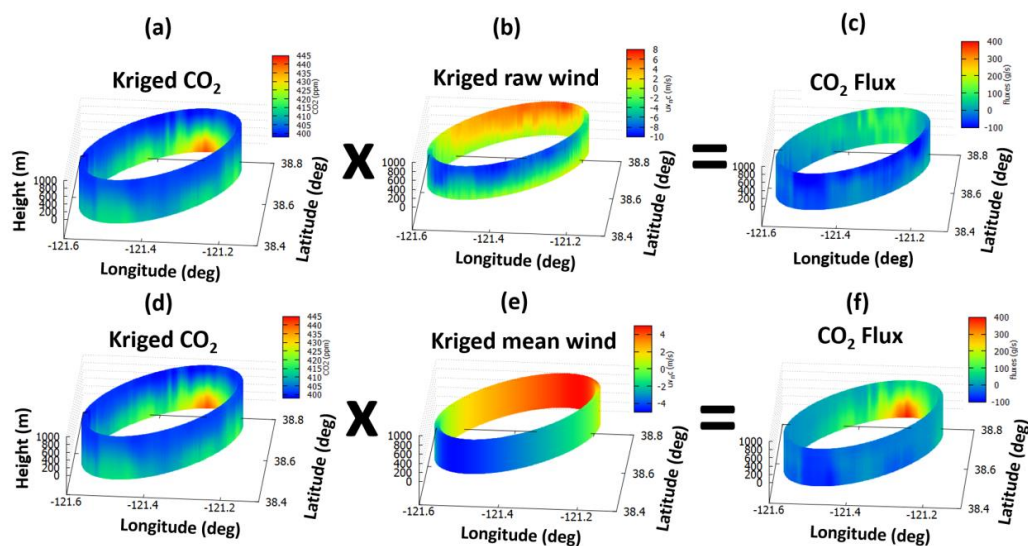


Figure 5: (a, d) Kriged CO<sub>2</sub> mixing ratio, (b) spatially varying raw measured wind, (e) mass balanced measured wind, (c) CO<sub>2</sub> flux using raw measured wind, (f) CO<sub>2</sub> flux using mass balanced wind on November 18, 2013. In panels (b, e), the blue color represents the inflow toward (and red outflow from) the cylinder so that it is defined as negative (positive) wind. The background CO<sub>2</sub> was chosen as the minimum mixing ratio at each vertical level.

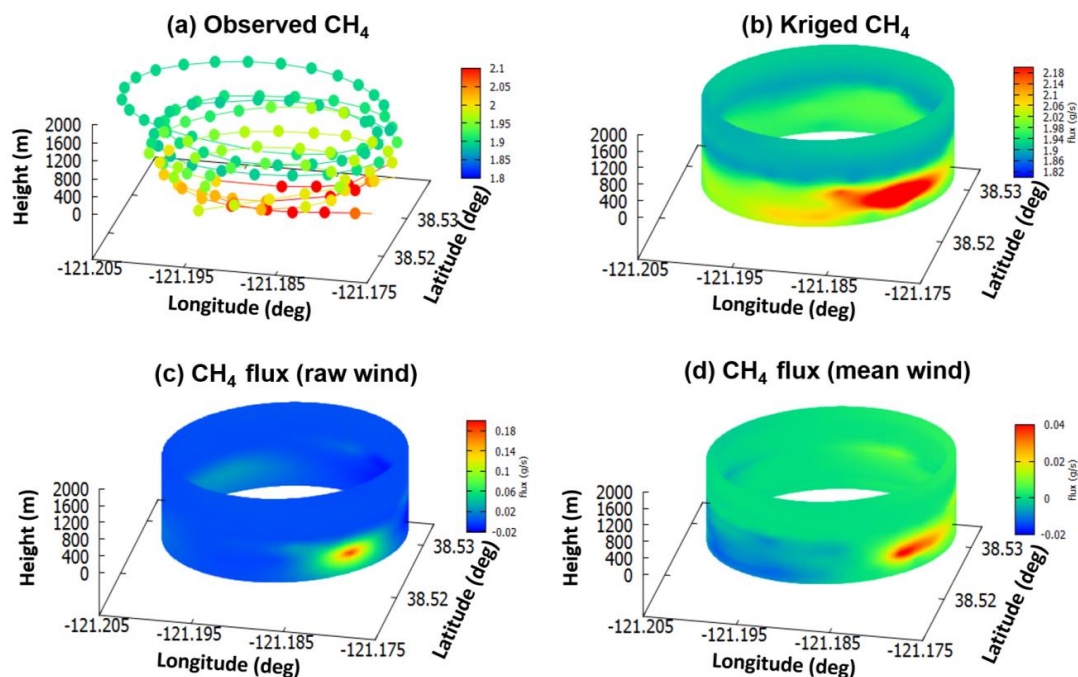


Figure 6: (a) The observed CH<sub>4</sub> mixing ratio, (b) the kriged CH<sub>4</sub> mixing ratio, (c) the CH<sub>4</sub> flux using raw measured wind, (d) the CH<sub>4</sub> flux using mass balanced mean wind (for each layer) over the landfill location on July 29, 2015. The fluxes in (c, d) are computed based on equation (2). The background value was chosen as the minimum value at each vertical level. The approximate diameter of the cylinder is 3 km.

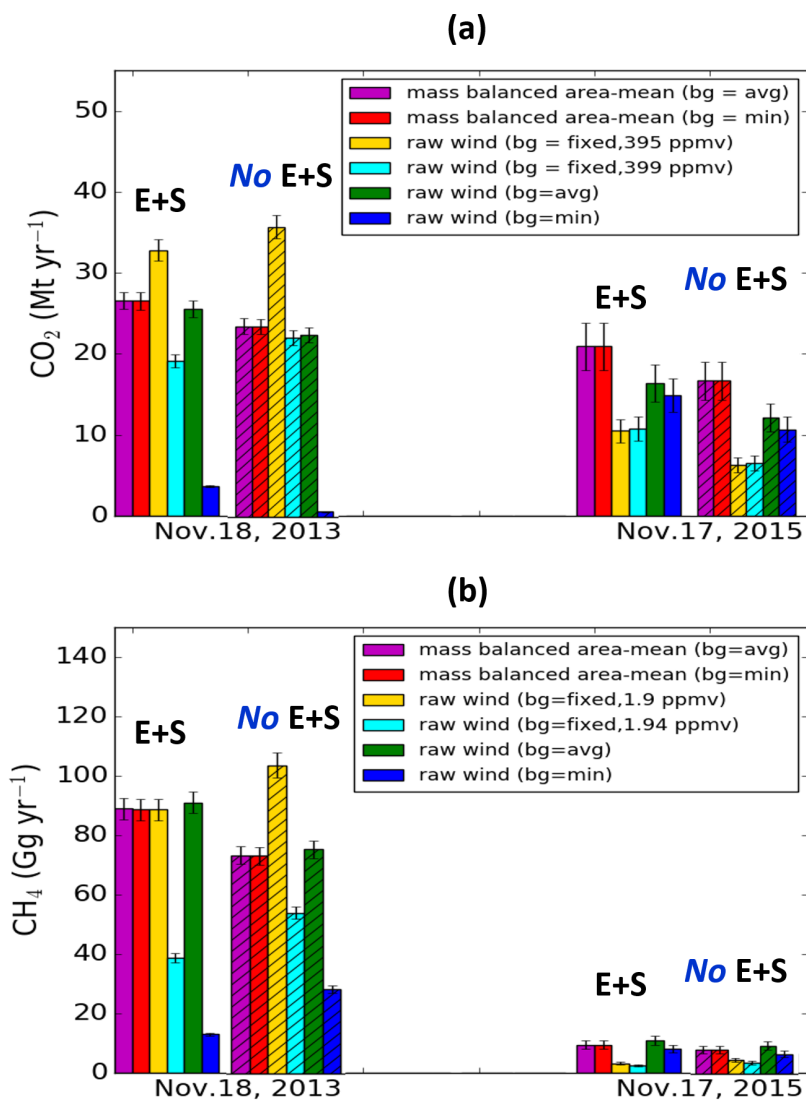


Figure 7: Urban-scale (a)  $\text{CO}_2$  [ $\text{Mt yr}^{-1}$ ] and (b)  $\text{CH}_4$  [ $\text{Gg yr}^{-1}$ ] emission rate estimates using raw wind and mass balanced area-mean wind, with different treatments of background values. Solid bars represent emission estimates with entrainment and surface flux (E+S), and hatched bars represent the corresponding emission estimates without consideration of entrainment and surface flux (No E+S). Error bars represent the uncertainty of the total emission fluxes. The average and minimum values for background are computed at each vertical level (about 7 meter interval), and the fixed value alternatives are 395 or 399 ppm for  $\text{CO}_2$  and 1.90 or 1.94 ppm for  $\text{CH}_4$  for all altitudes.



690

(a)

AJAX flight date		Urban Scale (large loop)			
		November 18, 2013		November 17, 2015	
		CO <sub>2</sub> (Mt yr <sup>-1</sup> )	CH <sub>4</sub> (Gg yr <sup>-1</sup> )	CO <sub>2</sub> (Mt yr <sup>-1</sup> )	CH <sub>4</sub> (Gg yr <sup>-1</sup> )
Mean wind	Bg= min	26.55±1.06	88.82±3.55	20.93±2.93	9.48±1.33
Mean wind	Bg=avg	26.58±1.06	88.99±3.56	20.92±2.93	9.51±1.33
Raw wind	Bg= min	3.68±0.15	13.00±0.52	14.92±2.10	8.16±1.14
Raw wind	Bg=avg	25.47±1.02	91.52±3.66	16.36±2.29	10.90±1.53

700

(b)

AJAX flight date		Local Scale (small loop): July 29, 2015			
		Landfill		Rice Field	
		CO <sub>2</sub> (Mt yr <sup>-1</sup> )	CH <sub>4</sub> (Gg yr <sup>-1</sup> )	CO <sub>2</sub> (Mt yr <sup>-1</sup> )	CH <sub>4</sub> (Gg yr <sup>-1</sup> )
Mean wind	Bg= min	0.22±0.08	7.83±2.74	0.25±0.04	2.63±0.45
Mean wind	Bg=avg	0.22±0.08	7.67±2.68	0.25±0.04	2.60±0.44
Raw wind	Bg= min	0.37±0.13	10.26±3.59	0.16±0.03	1.59±0.27
Raw wind	Bg= avg	0.22±0.08	8.13±2.85	0.25±0.04	2.66±0.45

710

**Table 1: The calculated CO<sub>2</sub> and CH<sub>4</sub> emission fluxes using different wind methodology (raw or mean wind) and different background values (minimum or average values at each level) for (a) urban scale on two different flight (November 18, 2013 and November 17, 2015) and (b) local scale on July 29, 2015. The vertical mass transfer (entrainment and surface flux) is taken into account.**

715